# Multi-energy microgrid ability to provide flexibility services to the system operator and security of supply to end-users

Tomislav Capuder, Matija Kostelac, Matej Krpan, Ivan Pavić
Department of Energy and Power Systems, Faculty of Electrical Engineering and Computing, University of Zagreb
10000 Zagreb, Croatia
E-mail: tomislav.capuder@fer.hr

***Abstract*—In the paper we propose a method to define the value of emergency service which the microgrid can provide both to the system operator and its own users. This means the microgrid operates as an energy community connected in parallel to the rest of the system and its operation is driven by market signals. However, it also needs to be able to detach from the main grid and maintain stable operation in the off-grid regime. To evaluate this, we demonstrate the following microgrid models: i) the on-grid mixed integer linear programming (MILP) model of a microgrid driven by market signals; ii) dynamic model of the microgrid during transitioning into island mode. From these models we define the boundaries/constraints later used in order to determine the monetary value of providing flexibility to the system operators and security of supply to end-users.**

***Index Terms*—ancillary services, islanding, microgrids, multi-energy systems, power system dynamics, microgrid stability**

## NOMENCLATURE

| | |
|---|---|
| Sets and Variables | |
| T, $t$ | Set and index of time steps |
| R, $r$ | Set and index of households |
| $P$ | Output power of heat pump |
| $XP$ | Binary variable indicating on/of state of heat pump |
| $CHP$ | Input power of CHP |
| $XCHP$ | Binary variable indicating on/of state of CHP |
| $H$ | Volume of energy stored in heat storage |
| $C, D$ | Charging and discharging power of batteries |
| $XC, XD$ | Indicate whether batteries are charging or discharging |
| $SoC$ | State of charge of batteries |
| $B, S$ | Volume bought and sold to the electricity market |
| Parameters | |
| $\mathrm{P_{min}}, \mathrm{P_{max}}$ | Minimum and maximum power output of heat pump |
| $\mathrm{CHP_{min}}, \mathrm{CHP_{max}}$ | Minimum and maximum power input of CHP |
| $\mathrm{H_{min}}, \mathrm{H_{max}}$ | Minimum and maximum capacity of heat storage |
| $\eta_{\mathrm{el}}, \eta_{\mathrm{th}}$ | Electric and heating efficiency of CHP |
| COP | Coefficient of performance for heat pump |
| $\mathrm{C_{min}}, \mathrm{C_{max}}$ | Minimum and maximum charging power of batteries |
| $\mathrm{D_{min}}, \mathrm{D_{max}}$ | Minimum and maximum discharging power of batteries |
| $\mathrm{SoC_{min}}, \mathrm{SoC_{max}}$ | Minimum and maximum SoC of batteries |
| $\eta_{\mathrm{C}}, \eta_{\mathrm{D}}$ | Charging and discharging efficiency of batteries |
| ED, HD | Electricity and heat demand of households |
| PV | Energy output of PV |
| $\mathrm{c^{el}}, \mathrm{c^{g}}$ | Price of electricty and gas |

## I. INTRODUCTION

In recent years European Union (EU) experienced rapid growth of installed renewable energy sources (RES). Due to their variability and unpredictability, system planning and operation has become significantly harder compared to the traditional system running. With the decentralization of production resources and democratization of investors into these sources, new models have emerged changing the known principles of operation, both in terms of services and time frame when these need to be provided. A vast number of papers researched microgrids as a concept where an energy community is self-sufficient, e.g. can operate in parallel to the system but more frequently supplies its demand while completely detached from the rest of the power system. Microgrid is a cluster of distributed energy sources, energy storage systems and controllable and uncontrollable loads, presented as a single entity towards the grid. Due to its relatively small-scale units, microgrid can rapidly change power in order to respond to system operator (SO) requests, and thus generate profit for its users. When properly dimensioned and run, microgrid can fulfill requests within minutes or even seconds from their annunciation. Presence of two energy vectors (heat and power) gives it additional flexibility in terms of ancillary services that can be offered. This paper models and analyses the ability of a multi-energy microgrid to provide response services to the SO in order to maximize the overall profit, especially when this request is relevant to system security and requests islanding of the microgrid.

Although there are numerous papers describing microgrid optimal unit sizing and dispatch on one side [1]–[3], and dynamics of microgrid on the other side [4], none of the papers connect these two aspects to define the value of microgrid constrained operation in order to provide security/resilience services to the SO and end-uses. Some papers consider islanding only as a different mode of operation, like [5] and [6], in which microgrid is disconnected from the grid and has to satisfy its own consumption. There are other papers that include islanding constraints in their optimisation like in [7]–[10]. The difference compared to our work, is that their islanding constraints ensure that production is equal to consumption, either by allocating enough capacity or by deferring load. None of them take into account frequency and voltage stability when transitioning to islanding mode. This paper connects optimal scheduling, dynamic stability and optimisation with islanding constraints and brings the

following contributions:

- Technical and economic evaluation of constrained multi-energy microgrid operation capable of operating both in on-grid and off-grid mode depending on the SO signals.
- The capability and the value of different multi-energy microgrid units to provide voltage and frequency stability services when called to transit into off-grid operational mode.

## II. Microgrid Modelling

The observed microgrid is a residential microgrid in which every household has a photovoltaic (PV) module and a battery storage. In addition, to satisfy heating demand, microgrid has a district heating system installed composed of a heat pump, combined heat and power (CHP) unit and thermal storage. Layout of the microgrid with all of its components is shown in Fig. 1.

The proposed model consist of three stages. The first and the third stages are optimization models based on mixed integer linear programming (MILP) while the second stage is a dynamic model described in section II-B. The optimization model in the first stage minimizes the cost of operation based on energy price signals. In the second stage, the model checks the stability of the microgrid during transitioning to island mode. Stability is tested for critical operating points in time, which are defined from the results of the first stage e.g. the hour when the microgrid has maximum export/import from the electric grid. As the result of the second stage, boundary conditions are defined for which the microgrid can safely transit into islanded mode operation. These boundary conditions are then translated into constraints and added to the first stage model and by doing this we obtain a new model calling it the third stage. The optimal scheduling is performed in order to define the monetary value of proving the security service to the end-users (or flexibility/security service to the system operator). This monetary value is calculated as the difference of objective function results in first and third stage.

### A. Optimization model

Equation (1) restrict minimum and maximum output power of the heat pump, (2) restrict input power of the CHP and (3) restrict amount of heat that can be stored. CHP is modeled with constant ratio between output electric and thermal power as shown in (4). Heat pump is considered as a ground-source with a constant coefficient of performance (COP). Electricity needed to extract heat from the ground is modeled with (5).

$$P^{\min} \cdot XP_t \leq P_t \leq P^{\max} \cdot XP_t \tag{1}$$

$$\mathrm{CHP}^{\min} \cdot XCHP_t \leq CHP_t \leq \mathrm{CHP}^{\max} \cdot XCHP_t \tag{2}$$

$$\mathrm{H}^{\min} \leq H_t \leq \mathrm{H}^{\max} \tag{3}$$

$$CHP_t^{\mathrm{el}} = CHP_t \cdot \eta_{\mathrm{el}},\ CHP_t^{\mathrm{th}} = CHP_t \cdot \eta_{\mathrm{th}} \tag{4}$$

$$P_t^{\mathrm{el}} = \frac{P_t}{\mathrm{COP}} \tag{5}$$

Standard linear model for battery storage system is shown in (6)-(10). Equations (6) and (7) limit minimum and maximum charging and discharging power, while (8) restrict charging and discharging of battery at the same time. Battery capacity or state of charge (SoC) is limited with (9) and is tracked with (10). Losses inside of batteries are defined with constant charging and discharging efficiency as shown in (10).

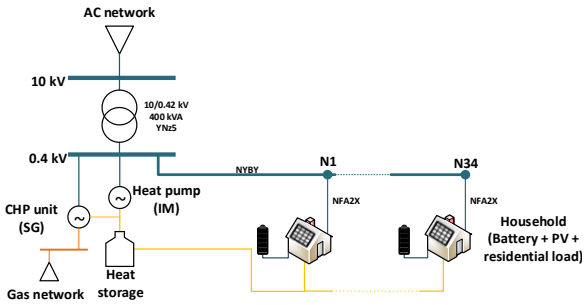


Fig. 1. Layout of the proposed microgrid

$$\mathrm{C}_r^{\min} \cdot XC_{r,t} \leq C_{r,t} \leq \mathrm{C}_r^{\max} \cdot XC_{r,t} \tag{6}$$

$$\mathrm{D}_r^{\min} \cdot XD_{r,t} \leq D_{r,t} \leq \mathrm{D}_r^{\max} \cdot XD_{r,t} \tag{7}$$

$$XC_{r,t} + XD_{r,t} \leq 1 \tag{8}$$

$$\mathrm{SoC}_r^{\min} \leq SoC_{r,t} \leq \mathrm{SoC}_r^{\max} \tag{9}$$

$$SoC_{r,t} = SoC_{r,t-1} + C_{r,t} \cdot \eta_{\mathrm{C}} - \frac{D_{r,t}}{\eta_{\mathrm{D}}} \tag{10}$$

Heating balance equation is defined with (11). Heat demand is increased to capture average loses in the heating system ($\eta_{\mathrm{HD}}$). The same equations tracks volume of stored heat in thermal storage. Electricity equilibrium is modelled with (12).

$$\sum_{i=1}^{R} \frac{\mathrm{HD}_{i,t}}{\eta_{\mathrm{HD}}} = (H_{t-1} - H_t) + P_t + CHP_t^{\mathrm{th}} \tag{11}$$

$$\sum_{i=1}^{R} \mathrm{ED}_{i,t} = \sum_{i=1}^{R} (D_{i,t} - C_{i,t} + \mathrm{PV}_{i,t}) - P_t^{\mathrm{el}} + CHP_t^{\mathrm{el}} + B_t - S_t \tag{12}$$

Objective of first and third stage is to minimise operational cost as shown in (13). Microgrid is paying for electricity and gas bought from market and it is getting paid for electricity sold to the grid.

$$(B_t - S_t) \cdot \mathrm{c}_t^{\mathrm{el}} + CHP_t \cdot \mathrm{c}^g \tag{13}$$

Third stage optimization has a few additional constraints that will result from second stage simulation and will be shown in section III.

### B. Dynamic model

The electrical model of the microgrid with the associated microgrid control system is modelled in DIgSILENT PowerFactory 2019. The grid is based on an actual low-voltage (LV) feeder in the distribution grid of Zagreb, Croatia. The transformer (Fig. 1) has short-circuit voltage $u_k = 4\%$. The main line from the LV feeder is a 1 kV 4x240 mm$^2$ NYBY

cable with $R = 0.136$ Ω/km and $L = 0.252$ mH/km, where $R$ and $L$ are positive sequence resistance and inductance per unit of length, respectively. Total length of the feeder line is approximately 600 m. Each household is connected to the main line through a 1 kV 3x35 mm$^2$ NFA2X cable with $R = 0.868$ Ω/km and $L = 0.264$ mH/km. The lengths of these connections to the main feeder line are in the range 10–20 m.

Residential loads are both dependent on voltage and frequency [11], [12], thus each household load is modelled as a dynamic load nonlinearly dependent on voltage and linearly dependent on frequency as described by (14)–(15) [13]:

$$P^{\mathrm{L}} = P_0(1 + k^{\mathrm{pf}}\Delta f)\left(\frac{U}{U_0}\right)^{n^{\mathrm{p}}} \tag{14}$$

$$Q^{\mathrm{L}} = Q_0(1 + k^{\mathrm{qf}}\Delta f)\left(\frac{U}{U_0}\right)^{n^{\mathrm{q}}}, \tag{15}$$

where $P_0$, $Q_0$ are initial load active and reactive power; $k^{\mathrm{pf}}$, $k^{\mathrm{qf}}$ are coefficients of active and reactive power frequency dependence; $U$, $U_0$ are load bus voltage and load bus initial voltage; $n^{\mathrm{p}}$, $n^{\mathrm{q}}$ are exponents of active and reactive power voltage dependence. Voltage and frequency dependence parameters are chosen according to [11], [12] as: $k^{\mathrm{pf}} = 0.9$ p.u., $k^{\mathrm{qf}} = -1.85$ p.u., $n^{\mathrm{p}} = 0.45$, $n^{\mathrm{q}} = 1.85$.

CHP unit is modelled as a detailed synchronous generator (SG) model (*Model 2.2* [14]) with a simple turbine-governor (*TGOV1* model [15] using parameters from [16]) and an excitation system (*AC5A* model [17] with default parameters in PowerFactory). Inertia constant of the generator is set to $H = 1.5$ s on the generator MVA base and the turbine-governor droop is set to $\sigma = 4\%$. All other parameters are given in the Appendix.

Heat pump is modelled as a 6-pole squirrel-cage induction motor (IM) directly connected to the grid with the mechanical torque quadratically proportional to the motor speed which is characteristic for various centrifugal pumps, fans and blowers. Parameters of the IM are given in the Appendix.

PV and battery systems are based on available models in PowerFactory [13] and are shown in Fig. 2 and Fig. 3, respectively. $P$ and $Q$ are measured active and reactive power to the grid, respectively. Asterisk (*) denotes a setpoint value. The inverters are controlled in grid voltage oriented reference frame. Current limiter, charge control and low-voltage ride through (LVRT) blocks do not have an impact on simulations in this paper, thus their description will be omitted for brevity (see [13] for more info). Moreover, only active power control loop is shown since $Q = 0 \iff i^{\mathrm{q},*} = 0$.

PV array model block (Fig. 2) outputs the maximum power point (MPP) voltage $U^{\mathrm{mpp}}$ and PV array current $I^{\mathrm{PV}}$ based on actual DC link voltage $U^{\mathrm{DC}}$ in V, solar radiation $E$ in Wm$^{-2}$ and ambient temperature $T$ in °C. PV array mode is described by (16)–(18) [13]:

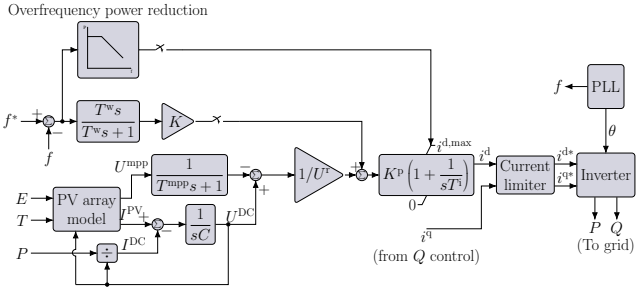


Fig. 2. Dynamic model of rooftop PV system

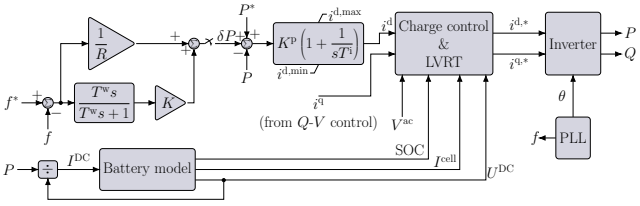


Fig. 3. Dynamic model of household battery system

$$U^{\mathrm{mpp}} = N_s k^{\mathrm{T,U}} U_0^{\mathrm{mpp}} \frac{\ln E}{\ln E_0} \tag{16}$$

$$I^{\mathrm{PV}} = N_p k^{\mathrm{T,I}} I_0^{\mathrm{sc}} \frac{E}{E_0}\left[1 - e^{\frac{N_s^{-1}U^{\mathrm{DC}} - U^{\mathrm{oc}}}{N_s^{-1}U^{\mathrm{mpp}} - U^{\mathrm{oc}}} \ln\left(1 - \frac{I_0^{\mathrm{mpp}}}{I_0^{\mathrm{sc}}}\right)}\right] \tag{17}$$

$$U^{\mathrm{oc}} = k^{\mathrm{T,U}} U_0^{\mathrm{oc}} \frac{\ln E}{\ln E_0}, \tag{18}$$

where $N_s$ is a number of modules in series that form a string and $N_p$ is the number of strings in parallel that form an array; $U_0^{\mathrm{mpp}}$, $I_0^{\mathrm{mpp}}$ are PV module maximum power point voltage and current at standard conditions ($E_0 = 1000$ Wm$^{-2}$); $U_0^{\mathrm{oc}}$, $I_0^{\mathrm{sc}}$ are PV module open-circuit voltage and short-circuit current at standard conditions, respectively; $k^{\mathrm{T,U}}$ and $k^{\mathrm{T,I}}$ are linear temperature correction factors for voltage and current, but these are equal to 1 since standard conditions are assumed ($T = 25°\mathrm{C}$).

Battery model block (Fig. 3) outputs the SoC, current of a single battery cell $I^{\mathrm{cell}}$ in A and battery terminal voltage $U^{\mathrm{DC}}$ in V based on the measured inverter power output and battery terminal voltage. Battery model is described by (19)–(21) [13]:

$$I^{\mathrm{cell}} = \frac{I^{\mathrm{DC}}}{N_p} = \frac{P}{N_p U^{\mathrm{DC}}} \tag{19}$$

$$\frac{U^{\mathrm{DC}}}{N_s} = U^{\max} \cdot SoC + U^{\min} \cdot (1 - SoC) - I^{\mathrm{cell}} \cdot R^{\mathrm{i}} \tag{20}$$

$$SoC = -\frac{1}{3600\kappa}\int_{t_0}^{t} I^{\mathrm{cell}}(\tau)d\tau, \quad SoC \in [0,1], \quad SoC \in \mathbb{R} \tag{21}$$

where $N_s$ is a number of battery cells in series that form a string and $N_p$ is the number of strings in parallel that form a battery; $I^{\mathrm{cell}}$ is the current of a single cell in A; $R^{\mathrm{i}}$ is

the internal resistance of the cell; $U^{\max}$, $U^{\min}$ are maximum and minimum permissible voltage of a battery cell in V, respectively; $\kappa$ is the rated cell capacity in Ah.

Grid frequency ($f$) support control layer is enabled or disabled by closing or opening the switches visible in Fig. 2 and Fig. 3. Battery has a combination of droop control and virtual inertia support, while PV has virtual inertia support (on the account of stored energy in the DC link) and power curtailment capability during overfrequency events. PVs and batteries are modelled as grid-feeding inverter-based sources using an averaged voltage source converter (VSC) model. In all cases the inverters are grid-feeding, i.e. the CHP unit is needed to define voltage and frequency. Operation in grid-forming mode is beyond the scope of this paper and is considered for future research.

Parameters of battery and PV units are given in the Appendix.

## III. Simulation and results

In the proposed microgrid there are 34 households. Each one has a battery storage system with charging and discharging power of 5 kW and capacity of 15 kWh. Energy efficiency of lithium ion batteries is usually expressed as a round trip efficiency (charging-discharging efficiency). With that in mind charging efficiency is set to 85% and discharging efficiency is 100% [18]. Additionally each household has a PV installed on its roof, each with power of 2.5 kW. District heating system has efficiency of 83% and is feed from a heat storage with a capacity of 400 kWh [19]. CHP has an input power of 350 kW. Electric efficiency and heating efficiency of CHP are 40% and 50%, respectively. Heat pump can output 65 kW of heat and has COP of 3.5. The sizes of units are defined as optimal sized based on optimal operational cost [20].

Optimisations in first and third stage have steps of one hour and in total there are 8760 steps (one year). For every optimisation step, parameters that have to be imputed are: electricity demand, heat demand, PV production and day ahead prices of electricity. Demand for electricity is generated using software from [21]. Heat consumption set for average American household were taken from [22] for city of Indianapolis, USA, because it has similar climate as Zagreb, Croatia [23]. The set was randomized to create a difference between households in the microgrid. Data sets for PVs are generated from [24]. Weather set for Zagreb, Croatia for year 2019 was taken and to ensure distinction between PVs, tilts and azimuths were changed in calculations. Day ahead prices of electricity were taken from ENTSO-E (European network of transmission system operators for electricity) transparency platform [25]. Gas price has singular average value of 15 euros per megawatt hour for every optimisation step.

### A. First stage: optimization

The result of the microgrid annual operational cost in the first stage is $-6.903$ euros, meaning that the microgrid is making profit by selling excess electricity in the day-ahead market. Two edge cases are chosen for stability analysis, maximum import and maximum export at the point of common coupling with the rest of the system. The case of maximum import (hour 8537) happened during the night when production of PVs is 0 and the price of electricity is very low, 8.3 euros per MWh. All batteries are being charged with maximum power of 5 kW, the heat pump is working on maximum power while the CHP is not producing. The total electricity load is 16.6 kWh. This leads to the import of 204.7 kWh. In the second case, maximum export in hour 1595, the situation is opposite. The chosen time step is in the middle of the day when PV production (46 kWh) and price of electricity (51.3 euros per MWh) are both high. Batteries are being discharged with power of 5 kW, the heat pump is not operational (high electricity prices) and the CHP is producing maximum amount of electricity and heat. Total electricity load is 6.1 kWh. Export to the grid is equal to 350 kWh.

### B. Second stage: dynamic stability

Characteristic operating points from the first stage (maximum import and maximum export) are checked to determine whether the microgrid can achieve stable transition to island mode, i.e. reach steady-state and satisfy voltage and frequency constraints. Since there are no standardized requirements for protection settings, values we used are based on practical experience from distribution systems and from [26], [27]: bus voltages are limited to $\pm 10\%$ of nominal value; RoCoF is limited to $\pm 2$ Hz/s measured over a 500 ms time window; frequency is limited to $\pm 2$ Hz in the first second after a disturbance after which the limit is set to $\pm 1$ Hz.

For each of the two operating points, three case studies are analyzed: i) only CHP unit provides frequency control, ii) batteries support CHP unit in frequency control and iii) batteries + PV support CHP unit in frequency control. In all cases, CHP unit controls voltage while batteries and PV operate with unity power factor. If an operating point is infeasible, then a feasible operating point which satisfies all constraints is iteratively found. New constraints are propagated back to the optimization model. Islanding is triggered at $t = 1$ s.

*1) Case I: only CHP unit controls frequency:* For maximum import, the first stage solution was infeasible because the system was unstable. To preserve stability and satisfy voltage and frequency constraints, maximum import must be limited to 68 kW and CHP size must be bigger than the import power, naturally. Results are shown in Fig. 4a–Fig. 4c.

For maximum export, the system is always unstable because PV production is larger than total load and there is not enough downward reserve. Thus the system would accelerate until protection trips it and power supply is lost. Only way to achieve stable operation is to curtail PV units manually.

*2) Case II: batteries support frequency:* If batteries participate in frequency support, then the operating point for maximum import from stage 1 is feasible. The system is stable and all voltage/frequency constraints are satisfied as shown in Fig. 5a–Fig. 5c.

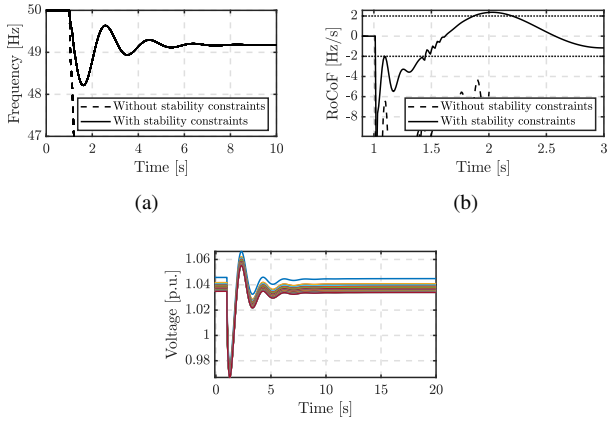


(a) (b) (c)

Fig. 4. Case I results for maximum import: (a) Frequency; (b) RoCoF; (c) Bus voltages in stable operation

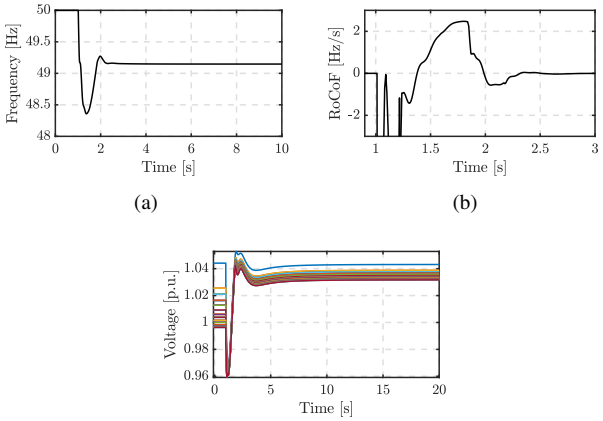


(a) (b) (c)

Fig. 5. Case II results for maximum import: (a) Frequency; (b) RoCoF; (c) Bus voltages in stable operation

The system is unstable for maximum export operating point from stage 1 regardless of the availability of batteries. The generation-load mismatch is too large so the system accelerates too quickly for the batteries to stabilize it. In order to preserve stability during islanding and satisfy voltage and frequency constraints, the export power has to be limited to 230 kW. Results are shown in Fig. 6a–Fig. 6c.

*3) Case III: batteries + PV support frequency:* The results for maximum import are the same as in the case when only batteries support frequency. This is because there is no PV production during maximum import. For maximum export, the system is stable for operating point from stage 1, but frequency and voltage limits are violated (Fig. 7). To satisfy them, maximum export is thus limited to 240 kW.

### C. Third stage: optimization

To ensure the microgrid is always capable of islanding we will implement additional constraints according to dynamic stability analysis. The goal of this stage is to minimise operational cost while satisfying constraints for dynamic stability.

*1) Case I: only CHP unit controls frequency:* In this case two new constraints are recognised for case of maximum import and zero for case of maximum export. Import from the market is restricted with $B_t \leq 68$ and CHP must have enough upward reserve to replace import (22). The results show a decrease in the annual microgrid profit of 12%, or more precisely $-6079$ euros.

$$B_t \leq \text{CHP}^{\max} \cdot \eta_{\text{el}} - CHP_t^{el} \tag{22}$$

*2) Case II: batteries support frequency:* When batteries are participating in frequency restoration, maximum import case is feasible so there is no need for restriction on import. On the other hand, export needs to be less than 230 kW ($S_t \leq 230$). This results in 3% higher cost ($-6700$ euros) that in first stage.

*3) Case III: batteries + PV support frequency:* Case III is very similar to case II. Export still needs to be restricted, but upper bound is set a bit higher to 240 kW. As expected result

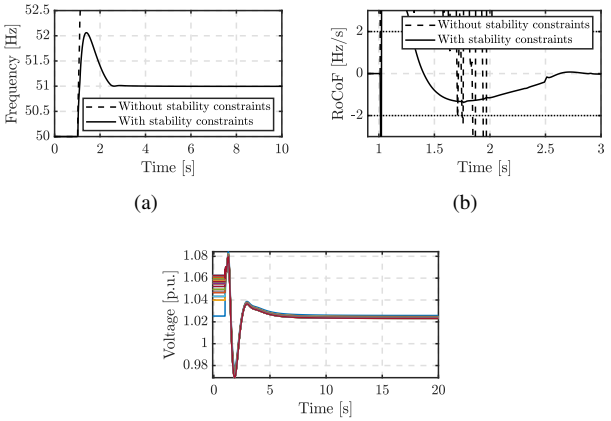


(a) (b) (c)

Fig. 6. Case II results for maximum export: (a) Frequency; (b) RoCoF; (c) Bus voltages in stable operation

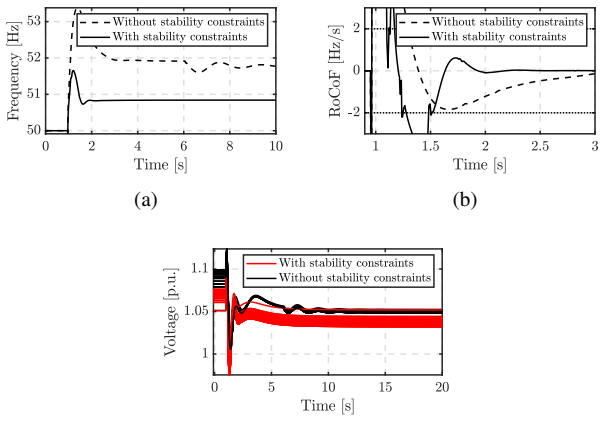


(a) (b) (c)

Fig. 7. Case III results for maximum export: (a) Frequency; (b) RoCoF; (c) Bus voltages

is lower operational cost of $-6744$ euros which is 2.4% more expensive than cost in first stage.

## IV. Conclusion

In this paper we propose a three stage model for optimising microgrid operation ensuring constant security of supply. Optimal operational points of the first stage are translated into the dynamic model of the second stage to define the boundary conditions of microgrid stable islanding. These conditions are further implemented in the third stage optimization algorithm to define the cost of having a continuous secure supply for microgrid end-users. Three case studies are defined in order to determine the value of having stability provided by household power electronic interface units. The results show that having domestic power electronics utilized as stability providers during microgrid islanding puts lower constraints on microgrid market operation as compared to relaying on conventional sources only. In fact, in the case where batteries and PVs provide stability, the additional constraints on microgrid market driven operation increase the operational cost by merly 2.4% as opposed to 12%, when this option is not used. Using domestic PV and battery storage system with power electronic control, microgrid was able to stay competitive on electricity market while being able to transition into islanding mode.

## Acknowledgment

The work is supported by Croatian Science Foundation (HRZZ) and Croatian Distribution System Operator (HEP ODS) under the project IMAGINE – Innovative Modelling and Laboratory Tested Solutions for Next Generation of Distribution Networks (PAR-2018-12). This work has been supported in part by the Croatian Science Foundation under the project WINDLIPS –WIND energy integration in Low Inertia Power System (grant No. HRZZ-PAR-02-2017-03).

## References

[1] C. Shilaja, T. Arunprasath, and P. Priya, "Day-ahead optimal scheduling of microgrid with adaptive grasshopper optimization algorithm," *International Journal of Communication Systems*, p. e4133, 2019.

[2] X. Yang, J. Long, P. Liu, X. Zhang, and X. Liu, "Optimal scheduling of microgrid with distributed power based on water cycle algorithm," *Energies*, vol. 11, p. 2381, 09 2018.

[3] N. Holjevac, T. Capuder, and I. Kuzle, "Defining key parameters of economic and environmentally efficient residential microgrid operation," *Energy Procedia*, vol. 105, pp. 999 – 1008, 2017, 8th International Conference on Applied Energy, ICAE2016, 8-11 October 2016, Beijing, China. [Online]. Available: http://www.sciencedirect.com/science/article/pii/S1876610217304794

[4] A. Karimi, Y. Khayat, M. Naderi, T. Dragičević, R. Mirzaei, F. Blaabjerg, and H. Bevrani, "Inertia response improvement in ac microgrids: A fuzzy-based virtual synchronous generator control," *IEEE Transactions on Power Electronics*, vol. 35, no. 4, pp. 4321–4331, 2020.

[5] S. Parhizi and A. Khodaei, "Market-based microgrid optimal scheduling," in *2015 IEEE International Conference on Smart Grid Communications (SmartGridComm)*, 2015, pp. 55–60.

[6] S. Parhizi, A. Khodaei, and M. Shahidehpour, "Market-based versus price-based microgrid optimal scheduling," *IEEE Transactions on Smart Grid*, vol. 9, no. 2, pp. 615–623, 2018.

[7] G. Liu, M. Starke, B. Xiao, X. Zhang, and K. Tomsovic, "Microgrid optimal scheduling with chance-constrained islanding capability," *Electric Power Systems Research*, vol. 145, pp. 197 – 206, 2017.

[8] A. Khodaei, "Microgrid optimal scheduling with multi-period islanding constraints," *IEEE Transactions on Power Systems*, vol. 29, no. 3, pp. 1383–1392, 2014.

[9] A. Khodaei, "Resiliency-oriented microgrid optimal scheduling," *IEEE Transactions on Smart Grid*, vol. 5, no. 4, pp. 1584–1591, 2014.

[10] Prakruti Shah and Bhinal Mehta, "Microgrid optimal scheduling with renewable energy sources considering islanding constraints," 2020.

[11] A. J. Collin, G. Tsagarakis, A. E. Kiprakis, and S. McLaughlin, "Development of low-voltage load models for the residential load sector," *IEEE Transactions on Power Systems*, vol. 29, no. 5, pp. 2180–2188, 2014.

[12] P. Kundur, *Power system stability and control*. McGraw-Hill, 1994.

[13] DIgSILENT GmbH, "Technical reference documentation," 2019.

[14] "IEEE Guide for Synchronous Generator Modeling Practices and Parameter Verification with Applications in Power System Stability Analyses," *IEEE Std 1110-2019 (Revision of IEEE Std 1110-2002)*, pp. 1–92, 2020.

[15] IEEE Task Force on Turbine-Governor Modeling, "Dynamic models for turbine-governors in power system studies," pp. 1–117, 2013, technical report PES-TR1.

[16] S. A. Papathanassiou and M. P. Papadopoulos, "Dynamic characteristics of autonomous wind–diesel systems," *Renewable Energy*, vol. 23, no. 2, pp. 293 – 311, 2001.

[17] "IEEE Recommended Practice for Excitation System Models for Power System Stability Studies," *IEEE Std 421.5-2016 (Revision of IEEE Std 421.5-2005)*, pp. 1–207, 2016.

[18] K. Li and K. J. Tseng, "Energy efficiency of lithium-ion battery used as energy storage devices in micro-grid," in *IECON 2015—41st Annual Conference of the IEEE Industrial Electronics Society*, 2015, pp. 005 235–005 240.

[19] R. Zwierzchowski and O. Niemyjski, "Influence of different operating conditions of a district heating and cooling system on heat transportation losses of a district heating network," *IOP Conference Series: Materials Science and Engineering*, vol. 471, p. 042019, 02 2019.

[20] T. Capuder and P. Mancarella, "Techno-economic and environmental modelling and optimization of flexible distributed multi-generation options," *Energy*, vol. 71, pp. 516 – 533, 2014.

[21] N. Pflugradt, "Load profile generator v8.9," https://www.loadprofilegenerator.de/, retrieved: 15.12.2019.

[22] Office of Energy Efficiency & Renewable Energy , "Commercial and residential hourly load profiles for all tmy3 locations in the united states," tinyurl.com/ybhrjuj6, retrieved: 15.12.2019.

[23] "Comparison of the Average Weather in Zagreb and Indianapolis," tinyurl.com/yavgewxm, retrieved: 15.12.2019.

[24] S. Pfenninger and I. Staffell, https://www.renewables.ninja/, retrieved: 13.01.2020.

[25] "ENTSO-E Transparancy platform: Day-ahead prices," tinyurl.com/y74f2cba, retrieved: 13.01.2020.

[26] H. J. Laaksonen, "Protection principles for future microgrids," *IEEE Transactions on Power Electronics*, vol. 25, no. 12, pp. 2910–2918, 2010.

[27] Salim Temtem and Karen Creighton, "Summary of studies on rate of change of frequency events on the all-island system," pp. 1–8, 2012, technical report.

## Appendix

Synchronous generator parameters: $S^{\mathrm{n}} = 176.2$ kW, $U^{\mathrm{n}} = 0.4$ kV; $\cos\varphi^{\mathrm{n}} = 0.8$

Induction motor parameters: $P^{\mathrm{n,mech}} = 100$ kW; $J$ = 8.2 kgm$^2$

*TGOV1* parameters: $T_1 = 0.05$ s; $T_2 = 0$; $T_3 = 0.5$ s; $D_t = 0$

PV parameters: $U_0^{\mathrm{mpp}} = 35$ V; $I_0^{\mathrm{mpp}} = 4.58$ A; $U_0^{\mathrm{oc}} = 43.8$ V; $I_0^{\mathrm{sc}} = 5$ A; $N_s = 16$; $N_p = 1$; $C = 1.5$ mF; $T^{\mathrm{mpp}} = 5$ s; $U^{\mathrm{r}} = 560V$; $K^{\mathrm{p}} = 10$; $T^{\mathrm{i}} = 0.01$ s; $T^{\mathrm{w}} = 1$ s; $K = 3$;

overfrequency power reduction: starts at 51 Hz, gradient: $-100$ %/Hz; $K^{\mathrm{p,PLL}} = 10$; $K^{\mathrm{i,PLL}} = 50$.

Battery parameters: $\kappa = 1$ Ah; $U^{\mathrm{min}} = 12$ V; $U^{\mathrm{max}} = 13.85$ V; $N_s = 36$; $N_p = 30$; $R^{\mathrm{i}} = 1$ m$\Omega$; $T^{\mathrm{w}} = 1$ s; $K = 10$; $R = 0.02$; $K^{\mathrm{p}} = 2$; $T^{\mathrm{i}} = 0.2$ s; $K^{\mathrm{p,PLL}} = 30$; $K^{\mathrm{i,PLL}} = 100$;